Demonstration of a Quartic Cell, a Free-Space True-Time-Delay Device Based on the White Cell

Carolyn M. Warnky, Rashmi Mital, and Betty Lise Anderson, *Senior Member, IEEE*

***Abstract*—The authors report on a design and demonstration of a quartic-style optical true-time-delay device based on a White cell. This device is designed for 81 sequential time delays with an incremental delay of 243 ps and a maximum delay of 19.683 ns. The time delays are implemented by free-space translations, with lens trains as needed for beam containment. A digital micro-electromechanical tilting micromirror array is used to send the light into different delay paths.**

***Index Terms*—Microelectromechanical devices, optical delay lines, phased array radar.**

I. Introduction

TRUE-TIME-DELAY devices (TTD) are of benefit in phased array antennas because they are frequency insensitive, therefore allowing a larger bandwidth than what is possible with phase shifters [1]. Electronic TTD devices have practical limitations due to the heavy and bulky implementations of coaxial cable, wave guides, or strip lines. These limitations can be reduced by using optical TTD devices [1].

For optical TTD, the RF signals from each antenna element are modulated onto light beams, which are then delayed individually as necessary for the appropriate steering of the antenna. The delayed beams are sent to high-speed photodetectors, where the RF signals are recombined, now with the correct relative phases.

There are two general types of optical TTD devices: free-space and guided-wave such as fiber delay lines. Guided-wave TTDs include planar waveguide styles [2], [3] that are optimal for very short delays. These typically use 1×2 switches to switch optical beams between planar waveguides of different lengths. Fibers of different lengths were also used early on [4]–[8]. These approaches in general require a series of delay lines for each antenna element or a single fiber for each delay and switching of beams among them. They are generally appropriate for long delays, but the fiber lengths must be cut extremely precisely or stretchers used to make the delay accurate. Alternatively, the errors can be corrected in the electronic TTDs that would be typically used for the short delays. More recently, fiber Bragg gratings [9], [10] and dispersive fiber [11]–[14] or prisms [15]–[18] have allowed the reuse of the same hardware for different elements, but they require either tunable lasers or multiple lasers with precisely controlled wavelengths. TTDs using free space generally enjoy the advantage of parallelism (many light beams share the same free space) [19]–[21], but long delays tend to lead to large volumes because of beam expansion. Other free-space approaches use traveling interference patterns, with spatial sampling [22] or holographic diffraction [23], and coupling of free-space beams into substrate hologram modes [24]. Free-space approaches generally do not require multiple or tunable lasers, and the time delays are not perturbed by dispersion.

We discuss here a free-space system that uses a single light beam for each antenna element, and has the advantage that hundreds or thousands of beams can circulate in the same volume, using a small amount of hardware. Our approach uses a White cell, which constantly refocuses the beam to avoid beam expansion, thus enabling very small volumes. Also, free-space lengths may be easily adjusted to fine tune the delays to the required accuracy.

The term "quartic" cell in this paper's title describes the counting system used in this White-cell-based delay device. In this case, the delays are counted in base "3" and is quartic in the sense that $3^4 = 81$ delays. The work described here differs from that of [25], in that it uses a digital microelectromechanical system (MEMS) with three discrete tip angles per mirror, rather than an analog one, for simpler control electronics. The digital MEMS also has smaller pixels and a smaller pitch for more compactness. Finally, multiple field lenses are used in the cell to reduce aberrations. Both systems are related to the earlier work described in [26].

In the following sections, we explain our free-space TTD device based on the White cell. In Section II, we present the development of the design from the original White cell. In Section III, we contrast two different designs for the quartic cell, and in Section IV, we report on experimental results for the most recent version of the quartic cell. We state some conclusions in the final section.

II. Background

A. White Cell

Our approach to optical TTD is based on a free-space optical configuration, which is first developed for long path lengths in spectroscopy by White [27]. Detailed descriptions of these White-cell-based designs are available elsewhere [25], [26], [28]–[32], so we only give a general outline here.

The White cell, which is shown from the top in Fig. 1(a), is an arrangement of three spherical mirrors, all with the same radius of curvature R. The mirrors are placed at the ends, facing inward, with two mirrors $Z1$ and $Z2$ on the right, and one mirror (mirror M) on the left side. Small input and output

Manuscript received November 8, 2005; revised May 30, 2006.

The authors are with the Department of Electrical and Computer Engineering, The Ohio State University, Columbus, OH 43210 USA (e-mail: Warnky.1@osu.edu; Mital.3@osu.edu; Anderson@ece.osu.edu).

Digital Object Identifier 10.1109/JLT.2006.881475

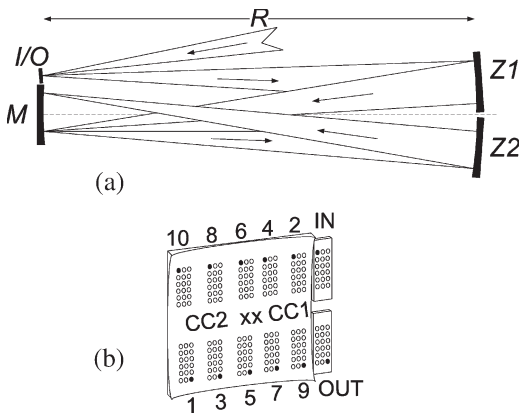

Fig. 1. (a) White cell. (b) Mirror M with spot patterns.

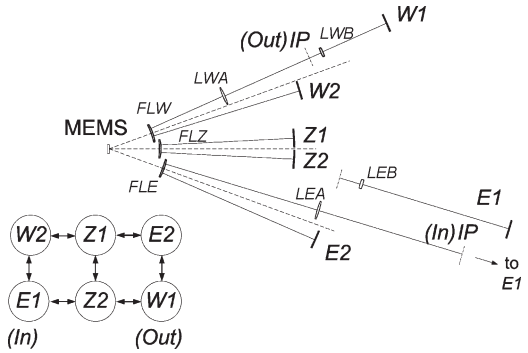

Fig. 2. Quartic cell with multiple field lenses.

turning mirrors lie at the side of mirror M. The length of the cell is R, so input spots are reimaged every round trip through the system. Two round trips are drawn in the figure.

The positions of the input beams, the initial angle of the input beams, and the locations of the centers of curvature determine the pattern of spots formed on M. An array of input beams can propagate through the system simultaneously, resulting in efficient use of space. A typical set of spot patterns is depicted in Fig. 1(b), where we see the front of mirror M, with the input and output turning mirrors on the right of M. The centers of curvatures of $Z1$ and $Z2$ are indicated by x's and the labels CC1 and CC2. One beam out of the array is highlighted, and the bounce numbers are printed above and below the outline of mirror M. The centers of curvature are slightly offset laterally from the center of M, thus allowing the beams to "walk off" M after a prescribed number of passes through the system. The beams then land on the output turning mirror and are redirected out of the system.

The White cell can be adapted for TTD in two types of architectures, which we call polynomial cells and exponential cells. These have been described elsewhere [25], [31], so here, we focus on the specific type of polynomial cell called the quartic cell. We next explain how this cell is adapted from the simple White cell.

B. Polynomial Cells

The first step in adapting the White cell for TTD is to replace mirror M with the optically equivalent flat reflecting surface and field lens. The surface is more than a simple mirror, because we need the capability to direct individual beams on different bounces to optical paths of various lengths. In the results reported here, the surface is a MEMS with an array of micromirrors, each with three tilt states. Each pixel in the array of micromirrors is individually controlled by computer interface and can tip to $\pm 10^\circ$ or flat.

We then combine multiple White cells having arms of different lengths, each sharing the MEMS surface but directed at angles determined by the tilt angles of the micromirror array. One cell, corresponding to the zero tip state, is designated as the null cell and has arms of equal length d_1. All beams experience a minimum delay of $n+1$ times the null-cell round-trip length, where n is the number of bounces for one beam on the MEMS surface. For additional delay, the beam is directed into the delay arms.

The parameters of polynomial cells are derived in detail in [25].[1] Some general results are given here. The number of states available in the MEMS or other spatial light modulator determines the number of delay arms p. The order of the system is also p, and the base is b, which is dependent on n and p. The number N of total sequential delays is proportional to b^p, although there will be some limitations for higher order cells. Each delay arm can be visited up to b $-$ 1 times, adding delay in each pass.

For the present quartic cell, of order four, the delay arms are longer than the null arms by Δ, $b\Delta$, $b^2\Delta$, and $b^3\Delta$, where Δ is the distance corresponding to half the minimum time-delay increment ΔT. The longest sequential delay is $(\mathrm{b}^4-1)\Delta T$ longer than the null delay, making N equal to b^4. In this configuration of the quartic cell, with $p=4$ and $n \in \{6, 10, 14\ldots\}$, the base is $b=(n+2)/p$.

In our implementation, there are ten bounces on the MEMS, giving a base of three with the longest delay being $80\Delta T$. The four delay arms introduce individual delays of Δ, 3Δ, 9Δ, and 27Δ. Any delay from 0 to 80Δ, in increments of Δ, can be selected by the appropriate combination of zero, one, or two trips to each of the delay arms.

The layout of the quartic cell is shown in Fig. 2, with a connectivity diagram in the lower left-hand corner. The MEMS plane and three field lenses are shown on the left, and the White-cell mirrors are shown on the right. The field lenses are labeled FLW, FLZ, and FLE, and the mirrors are labeled with the letters Z, E, and W, representing the zero, east, and west directions, respectively. There are additional lenses in arms $E1$ and $W1$, and the $E1$ arm is shown in two parts to reduce the width of the figure. The axes bisecting the pairs of mirrors are at 0° and $\pm 20^\circ$, or twice the tilt angle of the micromirrors. The White-cell mirrors are also labeled with numerals 1 or 2, designating whether that mirror's center of curvature is located at CC1 or CC2. The dashed lines labeled IP indicate image planes of the MEMS, which can be used for introducing input beams or extracting output beams

[1]Note that the number of bounces n is equal to $m+1$ in [3], because the output bounce is included in n.

A beam coming from any mirror labeled with a 1 will bounce off the MEMS and go to a mirror labeled with a 2, and *vice versa*. Only the null-cell mirrors can connect to three other mirrors; the delay-arm mirrors only have two choices for the next mirror. This is apparent in the connectivity diagram in the lower left corner of the figure where the circles represent the White-cell mirrors, and the double-headed arrows indicate bounces on the MEMS surface. Vertical arrows symbolize flat positions for the micromirrors, and the horizontal arrows refer to east or west tilts, which are determined by the E or W label on one of the connecting mirrors. The $E1$ arm is the input arm, and the $W1$ arm is the output arm.

The angles of the Z, E, and W mirrors must be precisely controlled to align the spot patterns on the micromirror array. Fortunately, these spherical mirrors only have to be aligned once. The micromirrors, which are rapidly tipped to multiple states, have a much looser angular alignment. The main design concern is that the mirrors in the delay arms have diameters large enough to intercept the complete beam for any inaccuracy of the micromirror tip angles [33]. The alignment of the input beams is also critical, both in position and angle.

The nature of any architecture of the White cell requires two imaging conditions to be satisfied: 1) M is reimaged for any round trip through the cell, and 2) the mirrors labeled with a 1 are conjugate to the mirrors labeled with a 2 for any valid trip through the cell. Both imaging conditions require a magnification of -1.

In Fig. 2, there are three separate field lenses to the right of the MEMS plane for the three different pairs of arms. It is also possible to have a single field lens. These two approaches are discussed in detail in the following section.

III. Quartic Cell: Two Approaches

A. Single Field Lens

Another polynomial cell design is the octic cell [25], [26], with N proportional to b^8. One implementation of the octic cell is two orthogonal quartic cells, and one of these quartic cells was demonstrated previously [25].

That quartic cell has a single field lens. The delay arms have different distances from the field lens to the White-cell mirrors to achieve time delay, so additional optics are necessary to satisfy the imaging conditions. The simplest solution is to add dielectric blocks, which can be chosen to give additional time delay and still achieve imaging [25], [32]. Another possibility is to add lenses in the delay path. This option is the best for very long delays, because the lens train constrains the diameter of the beam by continuously refocusing it. Lens trains also avoid the absorption losses and weight, which would result from long delays in blocks.

There is another less obvious difference between arms with delay blocks and arms with lens trains, and that is the image plane of the MEMS in a lens-train arm. With an image plane in the delay arm, input and output beams can be reflected through the delay arm instead of at turning mirrors next to the MEMS. This image plane is more convenient than the MEMS plane due to physical limitations in getting close to the MEMS. The pixel pitch in our current MEMS is 250 μm, making it extremely difficult to place an external turning mirror close enough to the outer pixel. Also, the entrance angle to the turning mirrors has to be even larger than the outer delay arm, and any input/output optics are difficult to place without interfering with other arms.

The single-field-lens design implemented previously [25] had three dielectric blocks and one lens train for the delay arms in the quartic cell. There, the lens-train arm was used for the input and output arrays, with the two arrays above and below each other.

That design, with one lens-train arm, reduces the number of delays possible for a given number of bounces, because the routing path has to start and end in the same arm. The delay-arm mirror in the I/O path and the mirror in the opposite corner of the connectivity diagram cannot both have $b-1$ visits in n bounces. For sequential delays, the longest delay with one lens train is $(b-1)*(b^3+1)+(b-2)*b$. In a ten-bounce quartic cell, the longest delay is reduced to $59\Delta T$. Alternatively, we can increase the number of bounces by two and have b^4+1 sequential delays.

B. Multiple Field Lenses

The multiple-field-lens design, as shown in Fig. 2, uses distances in air for the time delays. One of the delay arms for each field lens does not require additional optics beyond the field lens and the White-cell mirror. This is possible because the field lenses for the delay arms can be chosen with longer focal lengths than for the null cell, and the curvature of the White-cell mirrors is selected to work with that specific field lens to satisfy the imaging conditions. The other delay arm for each of the two outer field lenses has a lens train. These lens-train arms allow for input and output in separate arms, resulting in a true quartic cell with 81 delays in ten bounces on the MEMS.

By eliminating the dielectric blocks of the single-field-lens design, the amount of loss is lowered in each of the arms. This is obvious in the two arms without blocks or lenses. For the lens-train arms, there are some qualifications depending on the antireflection (AR) coating used and the material and thickness of the lenses or the blocks. In the previous cell, the dielectric blocks were made of BK7 and were intrinsically lossy, with about 1 dB for 1 ns of delay. If the blocks were fused silica, this could be reduced by a factor of about five for $\lambda = 1.55$ μm. A round trip through two lenses of fused silica with an AR coating of 99.75% transmission and thickness of 4 mm has a loss of less than 0.1 dB. The two longer delay arms have delays of 2.187 and 6.561 ns, so the lens trains have lower loss than blocks of either material.

The maximum loss, assuming dielectric mirrors ($R = 0.999$), no folding, AR-coating losses ($T = 0.9974$), and assuming 0.1-dB loss per bounce on the MEMS, is calculated to be 1.9 dB and the minimum is 1.5 dB (0.4-dB variation over the 81 possible delays). While this neglects input/output coupling and diffraction losses, a previous White cell [31] using the same MEMS (nine bounces, four bounces on the MEMS) had a worst case of 5.2-dB loss (measured). That demonstration had known diffraction issues due to undersized lenses, but in both cases, the loss of a real system is expected to be under 6 dB.

TABLE I
DISTANCES (IN MILLIMETERS) FOR THE QUARTIC CELL

Arm	T (ps)	D (mm)	d_0 (mm)	d_1 (mm)	d_2 (mm)	d_3 (mm)
W1	2187	328.1	123.1	215.0	286.8	187.5
W2	243	36.5	123.1	414.4		
Z1, Z2	0	0	138.8	362.0		
E1	6561	984.1	154.7	432.9	464.8	415.5
E2	729	109.4	154.7	454.8		

An additional advantage of using the multiple-field-lens design is reduced aberrations. The beams traveling to the delay arms go through the field lens at a maximum angle reduced by 20° compared to the single-field-lens case. This is twice the tip angle of the MEMS pixels, which was 10° in both cells. A cell could be designed for a MEMS array with a smaller tip angle, in which case, the difference would not be as important.

The newer quartic cell was also designed to be more compact than the previous version. This was partly due to the size of the micromirror arrays assumed for each design and partly due to the diameter of the field lenses. We used a standard of f/10 for the field lenses, but the diameter of the field lens in the single-field-lens design had to be larger because of the larger angles of the beams. The first quartic cell had a field-lens diameter of 60 mm, which was placed 25 mm from the MEMS plane, resulting in a null-cell distance d_1 of at least 600 mm to maintain f/10. The largest diameter field lens required for the second cell was 34 mm at a distance of 155 mm, resulting in a minimum d_1 of 340 mm (see [25] for information on calculating diameters). The actual lens used was 50.8 mm in diameter to fit standard mounts. The field lenses have to be farther away from the MEMS plane when using multiple field lenses compared to a single lens to allow the beams traveling to the different pairs of arms to be separated by the time they get to the field lenses.

The distances for the multiple-field-lens design are given in Table I. For each arm, the table lists the targeted time delay T, the corresponding distance in air D, assuming half of a round-trip pass, and the distances between the optical elements. The distances are labeled d_0 from the MEMS plane to the field lens, d_1 from the field lens to the White-cell mirror or the first lens in the lens train and d_2 and d_3 for the other distances in the lens train. The designed time delays were chosen to work with the optical elements within a target accuracy of ± 6 ps. As defined in Section II-B, the delay arms in order $W2$, $E2$, $W1$, and $E1$, have delays of Δ, 3Δ, 9Δ, and 27Δ, respectively, where Δ is 243 ps.

The optical elements are listed in Table II with the corresponding radii of curvature and thicknesses. All the measurements are given in millimeters. The field lenses are meniscus, and the lens-train lenses are biconvex. The curvatures were picked based on test plates available at a particular optics company.

C. Microelectromechanical Micromirror Array

We used a micromirror array designed and built by Sandia National Laboratories, which consists of a ten by ten rectangular array with 100-μm square mirrors on a 250-μm pitch. This array was originally designed for use in the octic cell, so it has two quadrants whose mirrors tip up and down, and two quadrants with mirrors that tip side to side or east and west. In the quartic cell, we can only use the two $E-W$ quadrants, giving a total of ten bounces for a five by one array of inputs. The mirrors tip in discrete angles of $\pm 10^\circ$.

TABLE II
OPTICAL SURFACES IN THE QUARTIC CELL

Lens/Mirror	R_1 (mm)	R_2 (mm)	thickness (mm)
FLW	-236.03	-110.9	4.5
FLZ	-235.0	-102.9	4.5
FLE	-412.64	-146.78	5.0
LWA	154.83	-154.83	5.0
LWB	97.43	-97.43	6.0
LEA	255.28	-255.28	4.0
LEB	216.03	-216.03	7.0
W1	-250.0		
W2, Z1, Z2	-600.0		
E1	-500.0		
E2	-700.25		

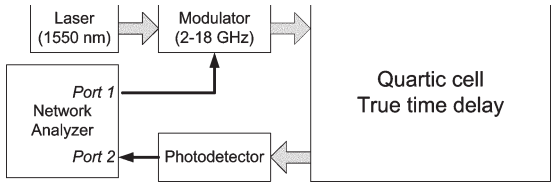

Fig. 3. Block diagram for time-delay measurements.

IV. EXPERIMENTAL RESULTS

We constructed the multiple-field-lens quartic cell of Fig. 2 and Tables I and II. Our primary experimental goal was to measure correct time delays for each of the arms. To measure delays, we connected the quartic cell as shown in Fig. 3. The gray arrows indicate optical inputs and outputs, and the black arrows represent RF signals. The light from the laser goes into the quartic cell after being modulated with an RF signal from the network analyzer. The photodetector receives the output optical beam and sends the resulting RF signal to port 2 of the network analyzer.

We measured the S_{21} parameter, which compared the input at port 2 to the frequency-swept RF output from port 1. An internal Fourier transform of the magnitude of the S_{21} parameter gave the time delay compared to the calibrated delay of the null cell. We found initially that the delays were not quite correct; for example, $W2$ was too short by 15.5 ps. The positions of the optics were adjusted to correct the time delay and still maintain focus. These arms were adjusted to the required delays within the precision of the measurement.

In Fig. 4, there are two sample time-delay measurements: one trip to arm $E1$ on the top and the null delay on the bottom. The vertical scale is 10 dB/div, and the horizontal scale is 2 ns/div,

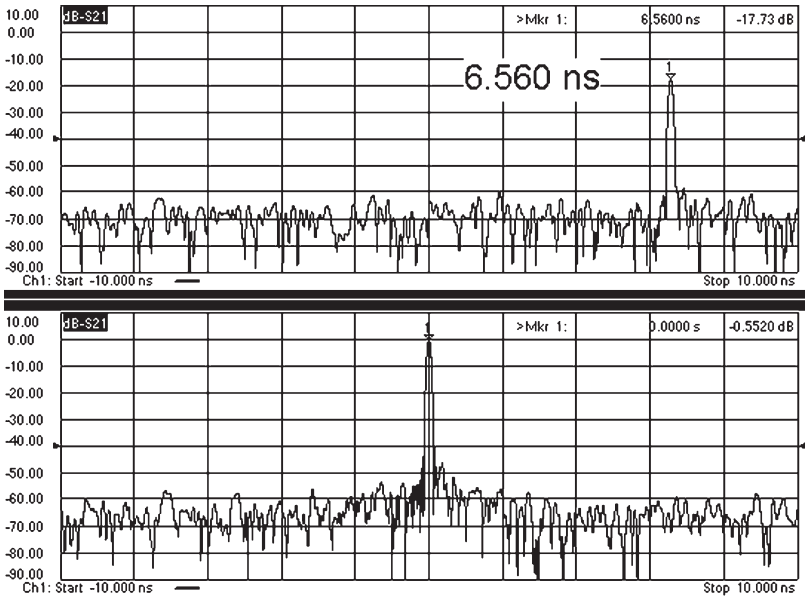

Fig. 4. Sample delay measurements of 6.56 ns (top) and zero delay (bottom).

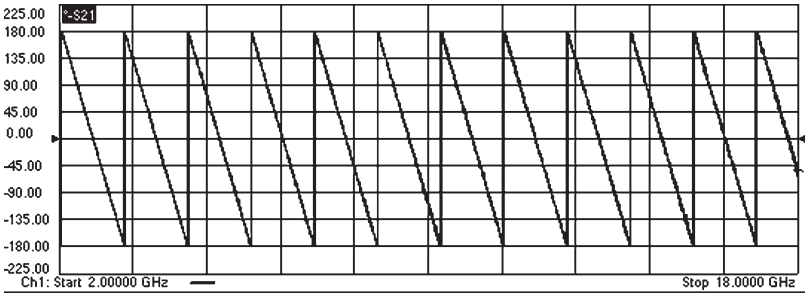

Fig. 5. Phase shift for 730 ps of time delay over 16-GHz bandwidth.

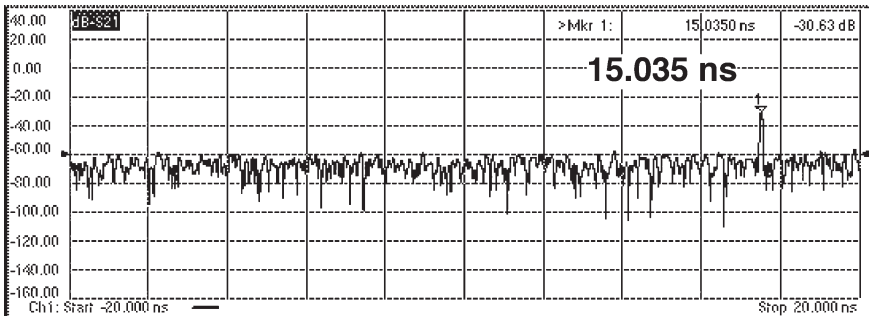

Fig. 6. Delay of 15.035 ns is obtained in two trips each to $W2$, $E2$, and $E1$.

extending from -10 to $+10$ ns. The targeted delay for arm $E1$ was 6561 ps (measured value 6560 ps), and the null delay was calibrated as zero. The measurement resolution was 1.25 ps. The noise floor was about -60 dB.

Fig. 5 shows the phase measurement for a time delay of 730 ps, with 45° of phase for each vertical division and 1.6 GHz for each horizontal division, extending from 2 to 18 GHz. As we can see, the phase shift is linear across the whole bandwidth, demonstrating the advantage of using the TTD.

In this quartic cell, the delays from 0 to 80Δ are obtained by sending each light beam to each of these four different delay arms either zero, one, or two times (counting in base 3). Fig. 6 shows a sample delay for multiple visits to different arms. These particular data were taken before the arm lengths were corrected. In this case, a light beam was sent to $W2$ twice (2x 227.5 ps), $E2$ twice (2x 730), and $E1$ twice (2x 6560) for a total delay of 15.035 ns. In all delays tested, multiple visits to delay arms added correctly within the measurement resolution. Therefore, we did not repeat all of the measurements when the individual arms were correctly tuned.

Table III lists the experimentally measured time delays for each delay arm after the final adjustments as well as the results from two different ways of measuring the power relative to the null delay. The column labeled "Peak" gives the peak power as read from the network analyzer, which is connected to a small-area high-speed photodetector. The last column gives the power

TABLE III
TIME DELAY AND LOSSES IN EACH ARM

Arm	T (ps ±1.25 ps)	Peak (dB ± 0.5dB)	Power (dB± 0.5dB)
W1	2188.8	-18.1	-9.9
W2	245.0	-5.0	-4.2
Z1, Z2	0.00	-0.5	-0.5
E1	6560.0	-17.7	-2.6
E2	728.75	-14.6	-4.4

measured on a large area detector, which has a slow response time. We were able to tune each of the arms to the correct time delay within the desired ±6-ps accuracy.

The small active area of the photodetector used for the time-delay measurements made it extra sensitive to alignment and focus. It was a New Focus 1417, with a detector radius of 10 μm. The larger area detector was a Newport 818-IR, with an active radius of 1.5 mm. The difference in alignment sensitivity accounts for the large discrepancy between the two columns of measurements in Table III. During initial measurements, arm $W2$ had a delay that was wrong by 15.5 ps and was sufficiently out of focus that the peak power was down by -22 dB. Getting that arm back into focus affected the input beam, also requiring adjusting its focus. In the process of refocusing the arms, the east arms dropped in power by more than 10 dB. Obviously, the system was not completely in focus in the final measurements given in Table III.

There were other experimental issues contributing to the measured loss. First, there were additional folding mirrors in the optical layout, which are not shown in the schematic of Fig. 2. We used dielectric coated mirrors in the null cell but had to use gold-coated mirrors in the other arms due to long lead times for the correctly sized dielectric-coated mirrors. Second, the coating on the right-angle mirrors used for the input and output turning mirrors did not extend all the way to the edges, especially to the top and bottom. The output turning mirror had to pick off a beam in the middle of the image plane because of the quadrants used on the MEMS. This meant the physical edge of the mirror extended into the path of the beams directed to mirror $W1$ for delay, contributing to the large loss in arm $W1$.

Another issue was the stability of the optical mounts, in particular, the fixtures holding the input turning mirror. We could see a drop off in power over a period of many minutes. As the different alignment and focusing adjustments are coupled together, it was not a trivial task to realign, and it could not be done in "real-time." This drop in power was seen even in the null cell, which was used as the calibrated power level for both the time-delay and power measurements. Between calibration and measurements, there was a drop of 0.5 dB, as listed in Table III.

V. SUMMARY AND CONCLUSION

We have presented an optical TTD device that can delay a signal from 0 to 19.683 ns in increments of 243 ps with accuracy of better than ±6 ps. This device is based on the White cell and uses free-space propagation for time delay. The switching for different delays is accomplished with a computer-controlled micromirror array, directing the optical beam into different arms as needed. The biggest advantage of the White-cell approach is its parallelism; many optical beams can circulate simultaneously in the same apparatus, and each can be individually controlled. Each one makes ten bounces in the apparatus. Further, only four delay paths have to be constructed to obtain 81 different delays, since the long delays are obtained by multiple visits to each delay arm. These same four arms are used by all the beams, which could be in the hundreds. Other advantages are lack of tunable lasers and the lack of dispersion in free space.

Switching into all delay arms was demonstrated, and various combinations of visits to the arms produced the desired delays. Importantly, we showed that the lengths of the delays can be made accurate to the required precision, which is an important advantage of a free-space system.

One area for future work is reducing loss further. Due to the nature of the White cell, the output is sensitive to the displacement of the input beam and of the centers of curvature of the White-cell mirrors. Stability is especially important when the output is sent to a high-speed photodetector with a small active area. The focus of each arm is also important because a blurred spot means less power on a small detector.

Alignment stability is an obvious concern for a free-space system such as this one that relies on imaging spots onto small pixels. The apparatus demonstrated here was intentionally made large for ease of experimentation, but a practical system would be built differently. In a later design, we have generated a baseline quartic-cell model with similar specifications (81 delays, maximum delay about 20 ns) in a volume approximately $10.5 \times 1.1 \times 2.75$ in (optics only, mounts not included). It uses a single field lens and a combination of dielectric blocks for short delays and folded mirror trains for long delays. It supports 160 light beams in this greatly reduced volume. The required White-cell-mirror alignment angle accuracy is 10 μrad, which is easily achieved with catalog mounts. In a non-laboratory environment, vibration and temperature excursions will need to be addressed, for example, by fabricating the entire assembly on a material of low thermal coefficient of expansion, and by aligning and then gluing the mirrors in place.

ACKNOWLEDGMENT

The authors would like to thank O. B. Spahn and B. Cowan at Sandia National Laboratories for the MEMS chip used in these experiments and S. A. Collins, Jr. for his comments and suggestions.

REFERENCES

[1] H. Zmuda and E. N. Toughlian, "Photonic aspects of modern radar," in *The Artech House Optoelectronics Library*, B. Culshaw, A. Rogers, and H. Taylor, Eds. Norwood, MA: Artech House, 1994.

[2] B. Kanack, M. Boysel, C. Goldsmith, C. Menni, G. Magel, and C. Takle, "Optical time delay network for phased arrays," in *Proc. Transition Opt. Processors Into Syst.*, 1993, pp. 114–132.

[3] L. Eldada, "Laser-fabricated delay lines in GaAs for optically steered phased-array radar," *J. Lightw. Technol.*, vol. 13, no. 10, pp. 2034–2039, Oct. 1995.

[4] D. D. Curtis and L. M. Sharpe, "True time delay using fiber optic delay lines," in *Proc. Int. Symp. Antennas and Propag.*, Dallas, TX, 1990, pp. 766–769.

[5] W. Ng and A. A. Watson, "The first demonstration of an optically steered microwave phased array antenna using true-time-delay," *J. Lightw. Technol.*, vol. 9, no. 9, pp. 1124–1131, Sep. 1991.
[6] A. Goutzoulis, K. Davies, J. Zomp, P. Hyrcak, and A. Johnson, "Development and field demonstration of a hardware-compressive fiber-optic true-time-delay steering system for phased-array antennas," *Appl. Opt.*, vol. 33, no. 35, pp. 8173–8185, Dec. 1994.
[7] V. Kaman, Z. Zheng, R. J. Helkey, C. Pusarla, and J. E. Bowers, "A 32-element 8-bit photonic true-time delay system base on a 288 × 288 3-D MEMS optical switch," *IEEE Photon. Technol. Lett.*, vol. 15, no. 6, pp. 849–851, Jun. 2003.
[8] J.-D. Shin, B.-S. Lee, and B.-G. Kim, "Optical true time delay feeder for X-band phased array antennas composed of 2 × 2 optical MEMS switches and fiber delay lines," *IEEE Photon. Technol. Lett.*, vol. 16, no. 5, pp. 1364–1366, May 2004.
[9] D. A. Cohen, Y. Chang, A. G. J. Levi, H. R. Fetterman, and I. L. Newberg, "Optically controlled serially fed phased array sensor," *IEEE Photon. Technol. Lett.*, vol. 8, no. 12, pp. 1683–1685, Dec. 1996.
[10] D. T. K. Tong and M. C. Wu, "Transmit-receive module of multiwavelength optically controlled phased-array antennas," *IEEE Photon. Technol. Lett.*, vol. 10, no. 7, pp. 1018–1019, Jul. 1998.
[11] H. Zmuda, E. N. Toughlian, P. B. Kanack, M. Boysel, C. Goldsmith, C. Menni, G. Magel, C. Takle, P. Payson, and H. W. Klumpe, III, "A photonic implementation of a wide-band nulling system for phased arrays," *IEEE Photon. Technol. Lett.*, vol. 10, no. 5, pp. 725–727, May 1998.
[12] O. Raz, R. Rotman, Y. Danziger, and M. Tur, "Implementation of photonic true-time delay using high-order-mode dispersion compensating fibers," *IEEE Photon. Technol. Lett.*, vol. 16, no. 5, pp. 1367–1369, May 2004.
[13] Y. Jiang, B. Howley, Z. Shi, Q. Zhou, R. T. Chen, M. Y. Chen, G. Brost, and C. Lee, "Dispersion-enhanced photonic crystal fiber array for a true time-delay structured X-band phased array antenna," *IEEE Photon. Technol. Lett.*, vol. 17, no. 1, pp. 187–189, Jan. 2005.
[14] D. B. Hunter, M. E. Parker, and J. L. Dexter, "Demonstration of a continuously variable true-time delay beamformer using a multichannel chirped fiber grating," *IEEE Trans. Microw. Theory Tech.*, vol. 54, no. 2, pp. 861–867, Feb. 2006.
[15] P. J. Matthews, M. Y. Frankel, and R. D. Esman, "A wide-band 4fiber-optic true time-steered array receiver capable of multiple independent simultaneous beams," *IEEE Photon. Technol. Lett.*, vol. 10, no. 5, pp. 722–724, May 1998.
[16] M. Y. Frankel and R. D. Esman, "Dynamic null steering in an ultrawideband time-steered array antenna," *Appl. Opt.*, vol. 37, no. 35, pp. 5488–5494, 1998.
[17] R. Taylor and S. Forrest, "Steering of an optically-driven true-time delay phased-array antenna based on a broad-band coherent WDM architecture," *IEEE Photon. Technol. Lett.*, vol. 10, no. 1, pp. 144–146, Jan. 1998.
[18] B. Vidal, D. Madrid, J. L. Corral, and J. Marti, "Novel photonic true-time-delay beamformer based on the free spectral range periodicity of arrayed waveguide gratings and fiber dispersion," *IEEE Photon. Technol. Lett.*, vol. 14, no. 11, pp. 1614–1616, Nov. 2002.
[19] D. Dolfi and P. Joffre, "Experimental demonstration of a phased-array antenna optically controlled with phase and time delays," *Appl. Opt.*, vol. 8, no. 26, pp. 1824–1828, 1996.
[20] H. R. Fetterman, Y. Chang, D. C. Scott, S. R. Forrest, F. M. Espiau, M. Wu, D. V. Plant, J. R. Kelly, A. Mather, W. H. Steier, and G. J. Simonis, "Optically controlled phased array radar receiver using SLM switched real time delays," *IEEE Microw. Guided Wave Lett.*, vol. 5, no. 11, pp. 414–416, Nov. 1995.
[21] N. A. Riza, "Polarization-based fiber optic delay lines," in *Proc. SPIE—Optical Technology for Microwave Applications VII*, 1995, vol. 2560, pp. 120–129.
[22] Y. Ji, K. Inagaki, O. Shibata, and Y. Karasawa, "Receive mode of optical signal processing multibeam array antennas," *IEEE Microw. Guided Wave Lett.*, vol. 8, no. 7, pp. 251–253, Jul. 1998.
[23] A. Kiruluta, G. S. Pati, G. Kriehn, P. E. X. Silveira, A. W. Sarto, and K. Wagner, "Spatio-temporal operator formalism for holographic recording and diffractions in a photorefractive-based true-time-delay phased-array processor," *Appl. Opt.*, vol. 42, no. 9, pp. 5334–5350, 2003.
[24] Y. Chen and R. T. Chen, "A fully packaged true time delay module for a K-band phased array antenna system demonstration," *IEEE Photon. Technol. Lett.*, vol. 14, no. 8, pp. 1175–1177, Aug. 2002.
[25] R. Mital, C. M. Warnky, and B. L. Anderson, "Design and demonstration of a higher order polynomial cell—Octic cell," *J. Lightw. Technol.*, vol. 24, no. 2, pp. 982–990, Feb. 2006.
[26] B. L. Anderson and R. Mital, "Polynomial-based optical true-time delay devices with microelectromechanical mirror arrays," *Appl. Opt.*, vol. 41, no. 26, pp. 5449–5461, Sep. 2002.
[27] J. White, "Long optical paths of large aperture," *J. Opt. Soc. Amer.*, vol. 32, no. 2, pp. 285–288, May 1942.
[28] B. L. Anderson, S. A. Collins, Jr., E. A. Beecher, C. A. Klein, and S. B. Brown, "Optically produced true-time delays for phased antenna arrays," *Appl. Opt.*, vol. 36, no. 32, pp. 8493–8503, Nov. 1997.
[29] B. L. Anderson and C. D. Liddle, "Optical true time delay for phased-array antennas: Demonstration of a quadratic White Cell," *Appl. Opt.*, vol. 41, no. 23, pp. 4912–4921, Aug. 2002.
[30] A. Rader and B. L. Anderson, "Demonstration of a linear optical true-time delay device by use of a microelectromechanical mirror array," *Appl. Opt.*, vol. 42, no. 8, pp. 1409–1416, Mar. 2003.
[31] B. L. Anderson, D. J. Rabb, C. M. Warnky, and F. M. Abou-Galala, "Binary optical true time delay based on the white cell: Design and demonstration," *J. Lightw. Technol.*, vol. 24, no. 4, pp. 1886–1895, Apr. 2006.
[32] S. Kunathikom, B. L. Anderson, and S. A. Collins, Jr., "Design and delay elements in a binary optical true-time delay device that uses a white cell," *Appl. Opt.*, vol. 42, no. 35, pp. 6984–6994, Dec. 2003.
[33] B. L. Anderson, V. Argueta-Diaz, F. Abou-Galala, G. Radhakrishnan, and R. J. Higgins, "Optical cross-connect switch based on tip/tilt micromirrors in a white cell," *IEEE J. Quantum Electron.*, vol. 9, no. 2, pp. 579–593, Mar./Apr. 2003.

Carolyn M. Warnky received the B.S. degree in electronic engineering from Southern Illinois University–Edwardsville, in 1979 and the M.S. and Ph.D. degrees in electrical engineering from The Ohio State University, Columbus, in 1994 and 2002, respectively.

She was a Postdoctoral Researcher with The Ohio State University at the time of this research.

Dr. Warnky is a member of the Optical Society of America.

Rashmi Mital received the B.Eng. degree from Nanyang Technological University, Singapore, in 1998 and the M.S. and Ph.D. degrees in electrical engineering from The Ohio State University, Columbus, in 2000 and 2005, respectively.

Her current research is in the development of true-time delay based on a recirculating (white) cell and micromirror technology. She recently had a paper published in the area of applied optics.

Betty Lise Anderson (S'79–M'90–SM'95) received the B.S. degree in electrical engineering from Syracuse University, Syracuse, NY, in 1978 and the M.S. and Ph.D. degrees in materials science and electrical engineering from the University of Vermont, Burlington, in 1988 and 1990, respectively.

She spent nine years in industry, including with Tektronix, Inc., GTE Laboratories, and Draper Laboratories. She is currently a Professor with The Ohio State University, Columbus, in the Department of Electrical and Computer Engineering. Her current research interests include analog optical signal processing, devices for optical communication systems, coherence, and semiconductor devices. She has coauthored (with R. L. Anderson) the *Fundamentals of Semiconductor Devices* (Burr Ridge, IL: McGraw-Hill, 2005).

Prof. Anderson is a member of the Optical Society of America. She is an Associate Editor for IEEE JOURNAL OF QUANTUM ELECTRONICS.